HEAT TRANSFER ENHANCEMENT IN INSERTED EXTRUDED ALUMINUM FINNED TUBES

by

Shifeng DENG, Huaishuang SHAO, Jian JIAO, Teng QU, and Qinxin ZHAO*

School of Energy and Power Engineering, Xi'an Jiaotong University

Original scientific paper
https://doi.org/10.2298/TSCI220708200D

Heat transfer enhancement in tubes is widely applied in various industrial processes. The traditional method of heat transfer enhancement is to insert radial fins to expand the internal surface area and destroy the flow. However, there is a flue gas corridor in the central area of the tube, and the cost of expanding the inner fin is high. A centrally symmetrical bent extruded aluminum fin was developed to enhance the heat transfer in the tube. An experimental platform was constructed to test the performance of inner finned tubes and explore the process of combining extruded aluminum inner fin with steel tube. The bent extruded aluminum fins with two side fins extending to the central axis possesses the best comprehensive heat transfer performance. The heat transfer correlation of the optimal fin structure is $Nu = 0.864Re^{0.4275}Pr_y^{0.3818}(Pr_y/Pr_w)^{-0.1004}$*. With low cost and strong heat transfer performance, the bent extruded aluminum inner fin tube will gain wide applications in the engineering field.*

Key words: *extruded aluminum inner fins, centrosymmetric, bent fins, steel-aluminum composite*

Introduction

Heat transfer enhancement in tubes have been widely applied in various industrial processes, such as the petroleum, chemical industry, metallurgy, electric power, and steam industries. The instruments include fire tube boilers, tube gas-gas heat exchangers, and solar collectors. The traditional in-tube heat exchange structure is a smooth tube structure, with the advantages of a simple structure, strong pressure bearing capacity, and low manufacturing cost. The enhanced heat transfer methods in the tube can be divided into three types: pressing the thread, adding a spoiler in the tube, and expanding the inner surface. Pressing the thread is threaded structures pressed on the smooth pipe, adding a spoiler is the spoiler inserted into the tube, and expanding the inner surface is to increase the internal heat transfer area of the tube. All three enhancement methods can destroy the flow boundary-layer in the tube, which have been the subject of extensive study. According to the number of thread lines, pressing the thread can be divided into hexagonal star, triangle, two-angle and coils. Jin *et al*. [1] and Kareem *et al*. [2, 3] studied the heat transfer and resistance characteristics of hexagonal star, triangle, and two-angle threaded pipes. Zachar [4] and Jayakumar *et al*. [5] studied the heat transfer and resistance characteristics of threaded coils. Aroonrat *et al*. [6], Weian *et al*. [7], Zhiguang *et al*. [8], and Guodong *et al.* [9] proposed the heat transfer coefficient correlation formula of

* Corresponding author, e-mail: zhaoqx@mail.xjtu.edu.cn

pressed threaded coils smoke tubes by experimental means, the Nusselt number of the threaded smoke pipe is 80-130% higher than that of the smooth tube at the same Reynolds and Prandtl numbers. Yuan *et al*. [10], Lesage *et al*. [11], Garcia *et al*. [12], and others studied the heat transfer and resistance characteristics of various spoilers added to the smoke pipe. The two strengthening methods of the thread and inner spoiler do not increase the effective heat exchange area, and the total strengthening capacity is limited. Expanding the inner surface strengthening can increase the heat exchange area in the tube by more than two times. Expanding the inner surface was sorted into two categories, radial and non-radial fins, according to the direction of the inner fins. Hosseinzadeh *et al*. [13], Tijing *et al*. [14], studied the strengthening effect of various star radial inner fins. Duan *et al*. [15] used a combination of numerical simulation and experiment to study the flower cluster radial heat transfer and drag characteristics of inner fins. Bellos *et al.* [16] studied the combined strengthening of radial inner fins and central spoilers. Bellos *et al*. [17], Meyer and Olivier [18], Naphon [19], and Al-Sarkhi and Abu-Nada [20] studied the influence of the height and number of straight radial inner fins on the heat transfer. Zeng *et al*. [21], Wang *et al.* [22], and Lin *et al*. [23] studied various continuous folded radial inner fins heat transfer characteristics of the fins. He *et al*. [24] studied the strengthening effect of helical inner fins and found that four helical fins have better comprehensive performance than eight. Maakoul *et al*. [25] studied the spiral double-tube heat exchanger and the longitudinal fin double tube. Searle *et al*. [26] studied the strengthening effect of the columnar inner fin, and the heat transfer coefficient increased by 132% compared with the plain tube. All radial fins had a large-scale central high temperature area. Kasperski andd Nems [27] compared the comprehensive performance of the plain, radial finned, annular, and axisymmetric finned tubes, the axisymmetric fins tube with 6-8 rows had the best heat transfer and resistance performances. The non-radial axisymmetric inner fins can eliminate the large-scale central high temperature area and divide the tube into flue gas channels that are similar to flat tubes. Peyghambarzadeh *et al*. [28], Nasr *et al*. [29], and Husein *et al*. [30] studied the enhanced heat transfer effect of the flat tube structure, and found that the best equivalent diameter of flat tube was approximately 11 mm. Therefore, non-radial inner fins have the best overall performance when the equivalent diameter of the smooth pipe is reduced to approximately 11 mm.

Non-radially inner fins exhibit excellent heat transfer performance. Non-radial fins have larger flow cross-sectional area and can eliminate the central high temperature zone. However, they are not widely used currently because of their high prices. In this study, a combination of experiment and numerical simulation was utilized to find the optimal non-radial fin structure, explore the process of combining extruded aluminum inner fin with steel tube and analyze the economy of fins.

Inner finned tube performance measurement test bench

As shown in fig. 1, the experimental bench comprises a diesel hot blast stove, an inner fin tube evaporator, and a centrifugal induced draft fan. The diesel hot blast stove produces 260-330 ℃ of hot flue gas, this flue gas is sent to the inner fin tube evaporator. Finally, flue gas is drawn out by the centrifugal induced draft fan. The inner finned tube evaporator contains an inner finned tube of 600 mm length, a shell, a large-diameter steam outlet, a water supply outlet, a water level gage*, etc.* The inner fin tube is replaced to measure the performance of tubes with different structures.The inner fin tube is composed of 150 mm long blank sections at both ends and 300 mm long fin segments in the middle. The inner fin tube is immersed in water, and the heat in the flue gas is taken away by water boiling and evaporation. The diesel fuel of the diesel hot blast stove is extracted from the diesel flask placed on the precision electronic scale, and the

diesel consumption is obtained by reading the change of the diesel quality per unit time. The temperature and pressure measuring points are set at the inlet and outlet of the 300 mm long fin segments to measure the inlet and outlet parameters of the flue gas. The total flue gas volume and flue gas composition can be calculated according to diesel consumption and oxygen ratio.

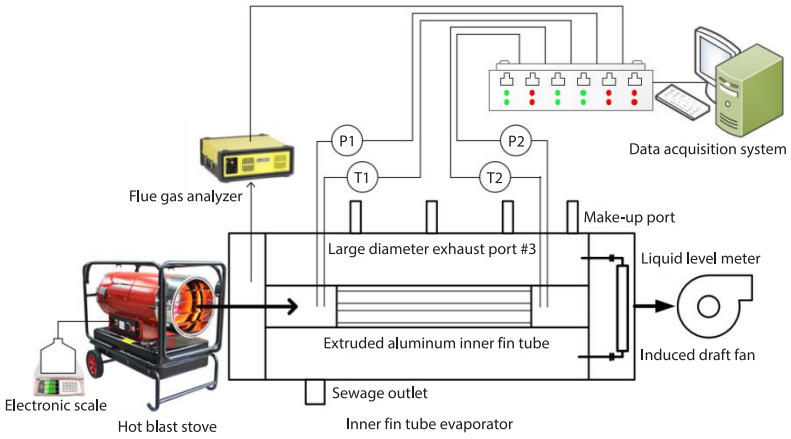

Figure 1. System diagram of inner finned tube performance measurement test bench

The pressure bearing capacity of extruded aluminum material is weak, and it is not resistant to acid and alkali corrosion. Thus, two pieces of extruded aluminum inner finned tubes are placed together and inserted into the steel pipe by interference fit to serve as the internal expansion heating surface, as shown in fig. 2. The interference fit refers to that the outer diameter of the inner extruded aluminum fin is larger than the inner diameter of steel tube, which can make the aluminum fin fit more closely with the steel tube. The inner fin is made of extruded aluminum material, and the thermal conductivity is 201 W/mK.

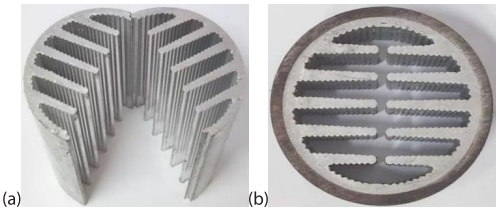

Figure 2. Schematic of axisymmetric inner fins; (a) two axisymmetric extruded aluminum inner fins and (b) axisymmetric extruded aluminum inner fin tube section after interference fit

During the experiment, by changing the fuel consumption of the diesel hot blast stove and the frequency of the centrifugal induced draft fan, the temperature and flow rate of the flue gas entering the evaporator of the inner fin smoke tube were changed.

Numerical and experimental simulation analysis

The FLUENT software was used to simulate the experimental 600 mm axisymmetric extruded aluminum inner fin tube. The ICEM software was utilized to process the geometry file of the smoke tube model. The maximum mesh size at the fin was set to 0.3 mm. A 3-D steady-state forced convection turbulence model was applied, and the physical parameters of the working substance in the tube were processed by a seven-point linear difference method. The standard k-ε model was used for the calculation, the second-order upwind style was selected to discretize the convection term, and the couple algorithm is used to solve the coupled problem of velocity and pressure. The boundary conditions of the calculation model were defined ignoring the thermal resistance of the steel pipe wall, water side, and the thermal resistance between the

steel tube and the axisymmetric interpolated extruded aluminum tube, the inner wall of the steel pipe was defined as a constant wall temperature-wall, and the inlet selected the velocity-inlet. The outlet selected the pressure-outlet. The interface between the axisymmetric interpolated extruded aluminum tube and the flue gas was defined as the coupled wall.

Figure 3 illustrates the five groups of experimental and numerical conditions. Shot peening and interference fit were adopted to eliminate the contact thermal resistance between the axisymmetric extruded aluminum inner fin and the steel tube. Shot peening utilized compressed air to carry the cast steel shot into the steel pipe to remove the oxide scale. Oxide scale in steel pipe will bring thermal resistance. The diameter of cast steel shot is usually less than 1mm. We trialed the heat transfer of the inner surface in the shot peening state and the original state. The outlet smoke temperature and resistance under shot peening condition was close to the result obtained by numerical simulation, which indicated that shot peening and interference fit can almost eliminate the thermal resistance.

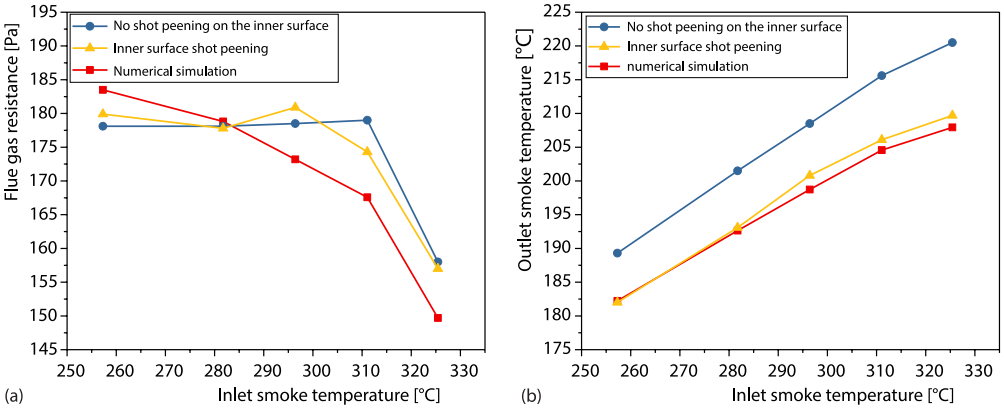

Figure 3. Comparison of inner surface without shot peening, inner surface shot peening, and numerical simulation; (a) resistance comparison and (b) temperature comparison

Equivalent diameter of interpolated extruded aluminum tube, D_h, is obtained:

$$D_h = \frac{4A_c}{P_c} \tag{1}$$

where A_c [m^2] is the cross-sectional area of axisymmetric inserted extruded aluminum pipe and P_c [m] – is the inner circumference of the section of axisymmetric interpolated extruded aluminum pipe.

The average temperature difference is obtained:

$$\Delta t_p = \frac{\left(t_j - t_s\right) - \left(t_j - t_c\right)}{\ln \dfrac{\left(t_j - t_s\right)}{\left(t_j - t_c\right)}} \tag{2}$$

where t_j [°C] is the inlet flue gas temperature of axisymmetric inner fin extruded aluminum tube section, t_c [°C] – the outlet flue gas temperature of axisymmetric inner fin extruded aluminum tube section, and t_s [°C] – the water side temperature of the inner fin tube evaporator.

The average convective heat transfer coefficient at flue gas side h_y is obtained using:

$$h_y = \frac{Q_y \rho_y C_p \left(t_j - t_c\right)}{3600 P_c l_c \Delta t_p} \tag{3}$$

where h_y [kWm^{-2}K^{-1}] and Q_y [m^3 per hour] are the standard condition flow of flue gas, ρ_y [kgm^{-3}] – the standard condition density of flue gas, C_p [kJK^{-1}kg^{-1}] – the specific heat capacity of flue gas, and l_c [m] – the length of an axisymmetric inner fin extruded aluminum tube.

Reynolds number is obtained:

$$\mathrm{Re} = \frac{u_y D_h}{\nu_y} \tag{4}$$

where u_y [ms^{-1}] is the flue gas-flow rate and ν_y [m^{2}s^{-1}] – the kinematic viscosity coefficient of flue gas.

The Nusselt number is obtained:

$$\mathrm{Nu} = \frac{h_y D_h}{\lambda_y} \tag{5}$$

where λ_y [kWm–1K^{-1}] is the thermal conductivity of flue gas. Five groups of experimental conditions are used as boundary conditions for numerical simulation. The variation between the Reynolds number and Nusselt number under the average flue gas-flow rate is shown in fig. 4. Because of the joint influence of the thermal resistance between the axisymmetric extruded aluminum inner fin tube and the steel tube and the thermal resistance of the steel tube wall thickness, the inner surface not shot peening condition in the experiment is weakened by an average of 18% compared with the numerical simulation condition. The error between the numerical simulation and the inner surface shot peening condition is less than 2.5%, indicating that the numerical model accurately reflects the actual heat transfer process.

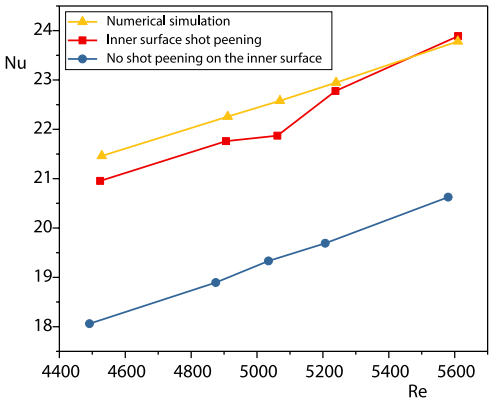

Figure 4. Nusselt number as a function of Reynolds number for the numerical simulation, inner surface shot peening, and inner surface unpeening

Optimization and improvement

Additional waves on the fin surface will promote heat transfer [31, 32]. The fin section of the axisymmetric extruded aluminum inner fin tube is added with alternating corrugations with a radius of 0.3 mm and 0.8 mm. Figure 5 shows the simulation results of adding corrugation and no corrugation on the fin surface. The addition of ripple has little effect on the overall change of heat transfer, and can slightly promote heat transfer. When ripples exist, the number of grids needs to be hundreds of millions. Therefore, the smooth plane is used to replace the corrugated plane to save computing resources.

The axisymmetric extruded aluminum inner fin tube with a smooth inner surface is denoted as tube #1, and the three newly proposed structures of center-symmetric bent fin tube are denoted as tubes #2, #3, and #4, tab. 1. As shown in fig. 6, the fins on both sides of tube #2 extend to the central axis; the fins on both sides of tube #3 are stacked upon each other, and the distance between the top diameters of the fins is 8 mm. the tops of the fins on both sides of tube #4 are separated from each other. The distance between the tops of the wings is 4 mm.

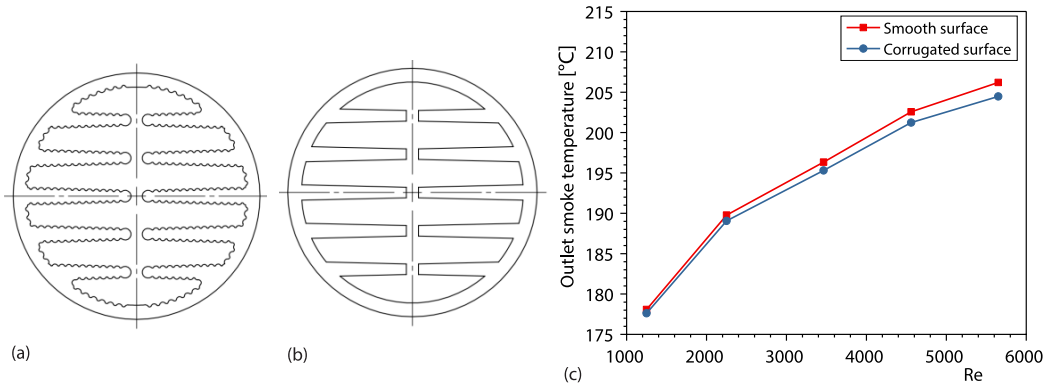

Figure 5. Influence of whether there is corrugation on the surface of extruded aluminum fins on heat transfer; (a) corrugated surface, (b) smooth surface, and (c) heat transfer performance comparison at different Reynolds numbers

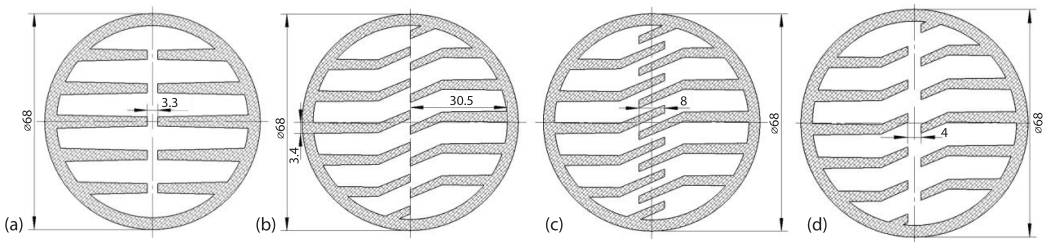

Figure 6. Four types of inner finned tubes: (a) #1, (b) #2, (c) #3, and (d) #4

Table 1. Parameters of four kinds of inner fin tubes

	Unit	#1	#2	#3	#4
Extruded aluminum sectional area	[mm^2]	1605.2	1529.2	1645.3	1468.19
Equivalent diameter	[mm]	12.3	11.2	9.3	12.4
Flue gas-flow area	[mm^2]	2026.4	2102.4	1986.3	2163.4
Heat exchange area of simulation section	[m^2]	0.196	0.224	0.254	0.208

The safe service temperature of extruded aluminum is 390 °C. To compare the heat exchange effect of these tubes #1 to #4 used as boiler flue gas tubes, the inlet flue gas temperature is set as 700 °C to prevent fins from being burnt by high temperature flue gas, and the flue gas-flow rates under inlet working conditions are 26 m/s, 23 m/s, 20 m/s, 17 m/s, 14 m/s, 11 m/s, 8 m/s, and 5 m/s. When the flue gas-flow rate is 17 m/s, the temperature cloud diagram of the four types of tubes is shown in fig. 7. High temperature areas of tube #1 and tube #4 intermittently distribute along the central corridor, while the fins of tube #2 and tube #3 cross each other and pass through the central high temperature areas. Subsequently, the advantages and disadvantages of the four types of tubes are further analyzed.

The numerical simulation results are shown in fig. 8. Under the same mass-flow, the outlet flue gas temperature of tube #3 is the lowest, but the resistance is also the largest. The outlet flue gas temperature of tubes #1 and #4 is similar. The outlet flue gas temperature of tube

#2 is lower than that of tubes #1 and #4, but the resistance of tube #2 is much lower than that of tube #3.

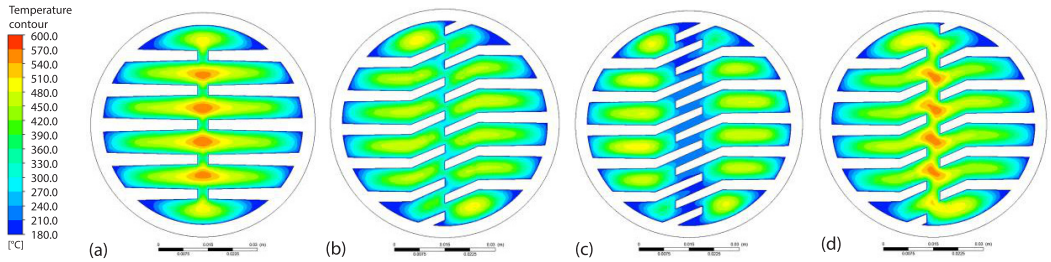

Figure 7. Temperature cloud map of the flue gas side at the outlet of the fin segments of the four inner fin tubes: (a) #1, (b) #2, (c) #3, and (d) #4

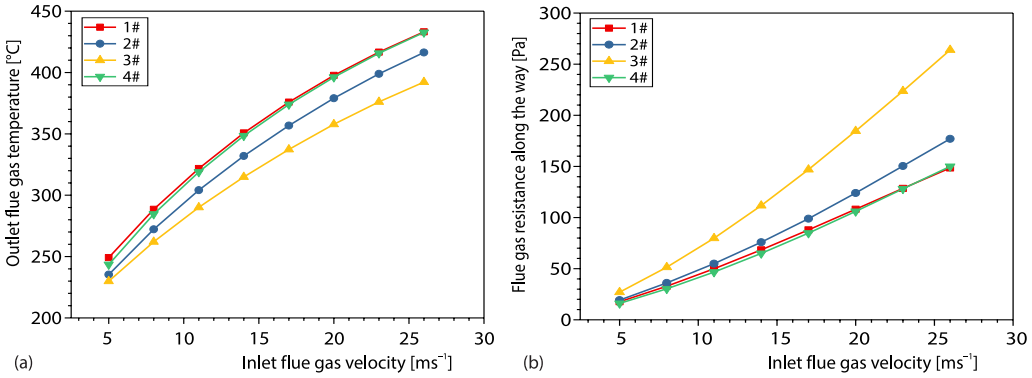

Figure 8. Flue gas temperature at the outlet of fin segments and resistance of fin segments for four inner fin tubes; (a) temperature and (b) resistance

The resistance coefficient of flue gas, f, uses the definition:

$$f = \frac{\Delta P_y D_h}{\frac{l_c \rho_y u_y^2}{2}} \tag{6}$$

where ΔP_y [Pa] is the resistance of extruded aluminum inner fin pipe section.

The heat transfer coefficient of flue gas, j, uses:

$$j = \frac{\mathrm{Nu}}{\mathrm{Re}\,\mathrm{Pr}^{1/3}} \tag{7}$$

where Pr is the Prandtl number of flue gas.

Equation (8) is used to describe the heat transfer difference for the same mass-flow.

$$\frac{\phi_{x\#}}{\phi_{1\#}} = \frac{\left(\frac{\mathrm{Nu} l_c P_c}{D_h}\right)_{x\#}}{\left(\frac{\mathrm{Nu} l_c P_c}{D_h}\right)_{1\#}} \tag{8}$$

Figure 9(a) exhibits the heat transfer difference for the same mass-flow. Tubes #4 and #1 have similar heat exchange capacities. Tubes #2 and #3 eliminate the central high tempera-

ture area distributed along the central axis, and the heat exchange capacity is significantly stronger than that of tube #1. The $j/f^{1/3}$ can describe the heat exchange capacity under the same pump work. As shown in fig. 9(b), although the heat exchange performance of tube #3 is improved by 21.2% on average, but $j/f^{1/3}$ is reduced by 15.8% on average. Therefore, the heat exchange performance is improved at the cost of increased resistance. The heat transfer performance of tube #2 is increased by 10.5% on average, whereas $j/f^{1/3}$ is reduced by 3.8% on average.

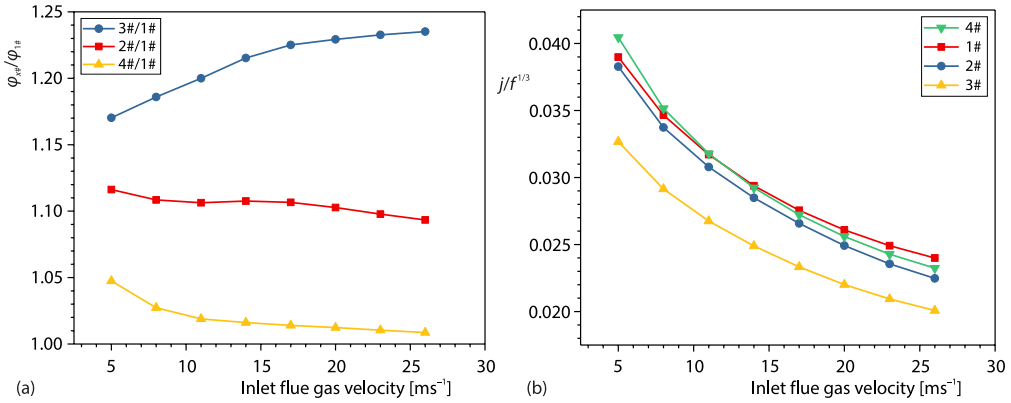

Figure 9. Comparison of heat transfer capacity at different conditions: (a) same mass-flow and (b) same flow rate

After the aforementioned analysis, tube #2 has the best comprehensive heat exchange performance. The surface of tube #2 is added with corrugations to expand the heat exchange area, and tube #2 is made, as shown in fig. 10(a). Because only part of the working conditions can be measured on the experimental bench, the final heat transfer characteristics of tube #2 are determined by a combination of numerical simulation and experimental verification. The main factors affecting the heat transfer performance of tube #2 are the inlet flue gas temperature l_y, the water side temperature t_w, and the inlet flue gas-flow rate u_{yj}. The inlet smoke temperature t_y selects 800 °C, 650 °C, 500 °C, 350 °C, and 200° C. The water side temperature t_w selects 220 °C, 180 °C, 140 °C, 100 °C, and 60 °C, and the inlet flue gas-flow rate u_{yj} is 20 m/s, 16 m/s, 12 m/s, 8 m/s, and 4 m/s. This amounts to a total of 125 sets of working conditions.

The heat transfer correlation is shown in eq. (9), and the correlation coefficient R^2 of the multiple linear regression fitting is 0.9875, where Pr_w is the Prandtl number of flue gas at water side temperature:

$$Nu = 0.8654Re^{0.4275}Pr_y^{0.3818}\left(\frac{Pr_y}{Pr_w}\right)^{-0.1004} \tag{9}$$

The resistance coefficient correlation formula is shown in eq. (10). The correlation coefficient, R^2, of the multiple linear regression fitting is 0.9233:

$$f = 33.643Re^{-0.7174}\left(\frac{Pr_y}{Pr_w}\right)^{16.2199} \tag{10}$$

As shown in fig. 10(b), the heat transfer performance was tested by the test bench. The steel-aluminum composite process will bring some thermal resistance. The experimental value at a low Reynolds number is lower than the numerical simulation calculation. At high Reynolds numbers, the flue gas-flow velocity in the tube is high, and each fin is a cantilever

beam structure, which will vibrate under the scouring of flue gas, the fin vibration disturbs the surface boundary-layer. The experimental value is gradually larger than the calculated value.

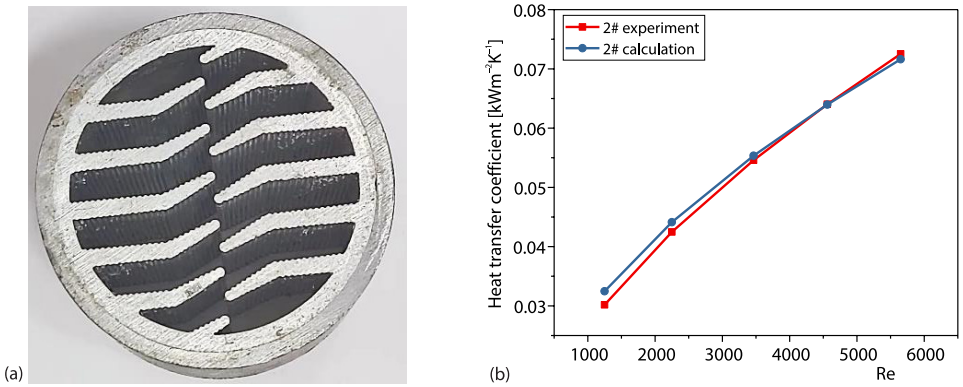

Figure 10. Sample, experiment and simulation results; (a) sample and (b) comparison of experimental and calculated heat transfer coefficients

Economic analysis

At the same flow rate, the heat transfer coefficient of the inner finned tube is converted to the heat transfer coefficient of the inner surface of the base tube, which is about five times that of the threaded tube and about 10 times that of the smooth tube. The inner fin tube has excellent heat transfer performance, but it has not been widely used due to economic factors. We have verified that shot peening and interference fit can almost eliminate the thermal resistance, the cost of these two processes is very cheap. Therefore, we compare the optimal inner fin structure with the traditional threaded smoke pipe for economy. Figure 11 shows the structure of the threaded smoke pipe, and tab. 2 lists the parameters of the two commonly used threaded smoke pipes #5 and #6.

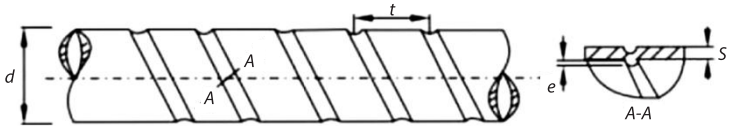

Figure 11. Schematic of the size of threaded smoke pipe

Table 2. Two threaded pipe size table

	Unit	*d*	*t*	*S*	*e*
Pipe #5	[mm]	76	40	4	2
Pipe #6	[mm]	51	40	3	2

The length and cost of the pipes required to complete the same heat exchange under the conditions of the same heat exchange temperature difference and the same resistance for the three types of pipes are calculated. The inlet flue gas temperature is 700 °C, the flue gas-flow rate is 16 m/s, the base pipe wall temperature is 180 °C, the number of #2 pipes is 20, and the outlet flue gas temperature is 500 °C, 450 °C, 400 °C, 350 °C, and 300 °C. First, the length, resistance, and weight of tube #2 are calculated under five working conditions according to eqs. (9) and (10). The resistances of tube #2 under five working conditions are 134.5 Pa,

150.1 Pa, 169.8 Pa, 196 Pa, and 236.1 Pa. Under the condition of keeping the resistance constant, the number and length of pipes #5 and #6 under five working conditions are calculated. Resistance coefficient f is calculated according to the eq. (11) of Li *et al.* [8] and the Nusselt number, is calculated by via eq. (12). When calculating the cost, the carbon steel amounts to 80 yuan per kg, the extruded aluminum is 500 yuan per kg, the steel-aluminum matching cost is 0.6 yuan per m, and thread pressing cost is 0.3 yuan per m. The calculation results are shown in fig. 12. The length and total price of the tube #2 are lower than those of pipe #6 and pipe #5:

$$\left(\frac{8}{\lambda}\right)^{0.5} = 2.5\ln\left(\frac{d}{2e}\right) + 0.868\left(\frac{e}{d}\right)^{-0.33}\left(\frac{t}{e}\right)^{0.366} \cdot \left[1 + 0.0296\left(\ln(\mathrm{Re}) - 9.48\right)^2\right]\exp\left(-0.005\frac{t}{e}\right) - 3.75 \tag{11}$$

$$\mathrm{Nu} = \frac{\mathrm{RePr}\left(\frac{\lambda}{8}\right)^{0.5}}{2.5\ln\left(\frac{d}{2e}\right) + 10.77\mathrm{Pr}^{0.5}\left(\frac{e}{d}\right)^{0.33}\left(\frac{t}{e}\right)^{0.096}\left(\frac{e}{d}\mathrm{Re}\left(\frac{\lambda}{8}\right)^{0.5}\right)^{0.273} - 3.75} \tag{12}$$

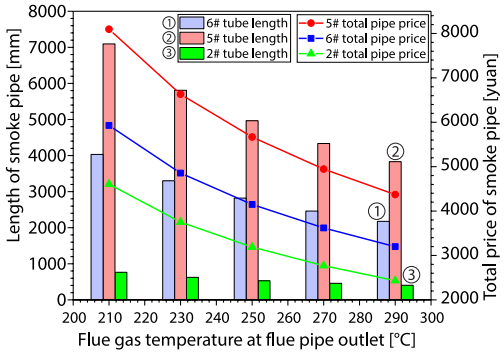

Figure 12. Economic comparison of pipes #5, #6, and #2 under five working conditions

Conclusions

We studied the heat transfer and resistance law of centrosymmetric inserted extruded aluminum fin. Our major findings are as follows.

- Shot peening and interference fit can almost eliminate the thermal resistance between the extruded aluminum fins and the steel pipe.
- Compared with the axisymmetric aluminum fin, the centrally symmetrical interpolated extruded aluminum fin can reduce the central high temperature zone.
- The extruded bent aluminum fins with two side fins extending to the central axis have the best comprehensive heat transfer performance. The heat transfer correlation of the optimal fin structure is $\mathrm{Nu} = 0.8654\mathrm{Re}^{0.4275}\mathrm{Pr}_y^{0.3818}(\mathrm{Pr}_y/\mathrm{Pr}_w)^{-0.1004}$. At the same flow rate, the heat transfer coefficient of the inner finned tube is converted to the heat transfer coefficient of the inner surface of the base tube, which is about 10 times that of the smooth tube. Under the condition of the same heat exchange and resistance, the length of the centrally symmetrical extruded aluminum fins is shorter than that of the threaded smoke pipe, and the cost is lower.

Acknowledgment

This work is supported by the Natural Science Foundation of China (No. 51876165) and the Key Research and Development Program of Shaanxi Province (2021GXLH-Z-005), which are gratefully acknowledged.

References

[1] Jin, Z.-J., *et al*., Effects of Pitch and Corrugation Depth on Heat Transfer Characteristics in Six-Start Spirally Corrugated Tube, *International Journal of Heat and Mass Transfer*, *108* (2017), Part A, pp. 1011-1025
[2] Kareem, Z. S., *et al*., Heat Transfer Enhancement in Two-Start Spirally Corrugated Tube, *Alexandria Engineering Journal*, *54* (2015), 3, pp. 415-422
[3] Kareem, Z. S., *et al*., Heat Transfer Enhancement in Three-Start Spirally Corrugated Tube: Experimental and Numerical Study, *Chemical Engineering Science*, *134* (2015), Sept., pp. 746-757
[4] Zachar, A., Analysis of Coiled-Tube Heat Exchangers to Improve Heat Transfer Rate with Spirally Corrugated Wall, *International Journal of Heat and Mass Transfer*, *5*3 (2010), 19-20, pp. 3928-3939
[5] Jayakumar, J. S., *et al.*, Experimental and CFD Estimation of Heat Transfer in Helically Coiled Heat Exchangers, *Chemical Engineering Research and Desig*n, *86* (2008), 3, pp. 221-232
[6] Aroonrat, K., *et al*., Heat Transfer and Single-Phase Flow in Internally Grooved Tubes, *International Communications in Heat and Mass Transfer*, *42* (2013), Mar., pp. 62-68
[7] Weiyan, Y., *et al*., Heat Transfer Calculation of Threaded Smoke Pipe, *Industrial Boiler*, *4* (2006), pp. 38-42
[8] Li, Z., *et al*., Seventeen-Year Technical Summary of the Development of New Water-Fired Tube and Shell Boilers, *Industrial Boiler*, *1* (2001), pp. 1-13
[9] Guodong, L., *et al*., Heat Transfer Characteristics of Air Cross-Flow for in-Line Arrangement of Spirally Corrugated Tube and Smooth Tube Bundles, *Journal of Zhejiang University SCIENCE*, *6* (2005), July, pp. 670-675
[10] Yuan, W., *et al*., Heat Transfer and Friction Characteristics of Turbulent Flow through a Circular Tube with Ball Turbulators, *Applied Sciences*, *8* (2018), 5, 776
[11] Lesage, F. J., *et al*., A Study on Heat Transfer Enhancement Using Flow Channel Inserts for Thermoelectric Power Generation, *Energy Conversion and Management*, *75* (2013), Nov., pp. 532-541
[12] Garcia, A., *et al.*, Experimental Study of Heat Transfer Enhancement in a Flat-Plate Solar Water Collector with Wire-Coil Inserts, *Applied Thermal Engineering*, *61* (2013), 2, pp. 461-468
[13] Hosseinzadeh, K., *et al*., Effect of Internal Fins along with Hybrid NanoParticles on Solid Process in Star Shape Triplex Latent Heat Thermal Energy Storage System by Numerical Simulation, *Renewable Energy*, *154* (2020), July, pp. 497-507
[14] Tijing, L. D., *et al*., A Study on Heat Transfer Enhancement Using Straight and Twisted Internal Fin Inserts, *International Communications in Heat and Mass Transfe*r, *3*3 (2006), 6, pp. 719-726
[15] Duan, L., *et al*., Flow and Heat Transfer Characteristics of a Double-Tube Structure Internal Finned Tube with Blossom Shape Internal Fins, *Applied Thermal Engineering*, *128* (2018), Jan., pp. 1102-1115
[16] Bellos, E., *et al.*, Enhancing the Performance of Parabolic trough Collectors Using Nanofluids and Turbulators, *Renewable and Sustainable Energy Reviews*, *91* (2018), Aug., pp. 358-375
[17] Bellos, E., *et al*., The Impact of Internal Longitudinal Fins in Parabolic trough Collectors Operating with Gases, *Energy Conversion and Management*, *135* (2017), Mar., pp. 35-54
[18] Meyer, J .P., Olivier, J. A., Transitional Flow Inside Enhanced Tubes for Fully Developed and Developing Flow with Different Types of Inlet Disturbances: Part I – Adiabatic Pressure Drops, *International Journal of Heat and Mass Transfer*, *54* (2011), 7-8, pp. 1587-1597
[19] Naphon, P., On the Performance and Entropy Generation of the Double-Pass Solar Air Heater with Longitudinal Fins, *Renewable Energy*, *30* (2005), 9, pp. 1345-1357
[20] Al-Sarkhi, A., Abu-Nada, E., Characteristics of Forced Convection Heat Transfer in Vertical Internally Finned Tube, *International Communications in Heat and Mass Transfer*, *32* (2005), 3-4, pp. 557-564
[21] Zeng, M., *et al.*, Effect of Lateral Fin Profiles on Stress Performance of Internally Finned Tubes in a High Temperature Heat Exchanger, *Applied Thermal Engineerin*g, *50* (2013), 1, pp. 886-895
[22] Wang, Q.-W., *et al*., Effect of Lateral Fin Profiles on Turbulent Flow and Heat Transfer Performance of Internally Finned Tubes, *Applied Thermal Engineering*, *29* (2009), 14-15, pp. 3006-3013
[23] Lin, M., *et al*., Laminar Heat Transfer Characteristics of Internally Finned Tube with Sinusoidal Wavy Fin, *Heat and Mass Transfer*, *47* (2011), 6, pp. 641-653

[24] He, Z., *et al*., Heat Transfer Enhancement and Exergy Efficiency Improvement of a Micro Combustor with Internal Spiral Fins for Thermophotovoltaic Systems, *Applied Thermal Engineering*, *189* (2021), May, 116723
[25] El Maakoul, A., *et al*., Numerical Investigation of Thermohydraulic Performance of Air to Water Double-Pipe Heat Exchanger with Helical Fins, *Applied Thermal Engineering*, *127* (2017), Dec., pp. 127-139
[26] Searle, M., *et al.*, Heat Transfer Coefficients of Additively Manufactured Tubes with Internal Pin Fins for Supercritical Carbon Dioxide Cycle Recuperators, *Applied Thermal Engineering*, *181* (2020), 116030
[27] Kasperski, J., M. Nems, Investigation of Thermo-Hydraulic Performance of Concentrated Solar Air-Heater with Internal Multiple-Fin Array, *Applied Thermal Engineerin*g, *58* (2013), 1-2, pp. 411-419
[28] Peyghambarzadeh, S. M., *et al*., Improving the Cooling Performance of Automobile Radiator with Al_2O_3/Water Nanofluid, *Applied Thermal Engineering*, *31* (2011), 10, pp. 1833-1838
[29] Nasr, M., *et a*l., Performance Evaluation of Flattened Tube in Boiling Heat Transfer Enhancement and Its Effect on Pressure Drop, *International Communications in Heat and Mass Transfer*, *37* (2010), 4, pp. 430-436
[30] Hussein, A., *et al*., Heat Transfer Enhancement with Elliptical Tube under Turbulent Flow TiO_2-Water Nanofluid, *Thermal Science*, *20* (2016), 1, pp. 89-97
[31] Nine, M., *et al*., Turbulence and Pressure Drop Behaviors Around Semicircular Ribs in a Rectangular Channel, *Thermal Science*, *1*8 (2014), 2, pp. 419-430
[32] Cho, C., *et al*., Numerical Investigation into Natural-Convection Heat Transfer Enhancement of Copper-Water Nanofluid in a Wavy Wall Enclosure, *Thermal Science*, *16* (2012), 5, pp. 1309-1316

Paper submitted: July 8, 2022
Paper revised: November 13, 2022
Paper accepted: November 14, 2022